MODELING DAMAGED WINGS - ELEMENT SELECTION AND CONSTRAINT SPECIFICATION

W. J. Stronge

Naval Weapons Center

INTRODUCTION

The NASTRAN analytical program has been primarily used for structural design. Nevertheless, no problems were anticipated in applying this program to a damaged structure as long as the deformations were small and the strains remained within the elastic range. In this context, NASTRAN was used to test three-dimensional analytical models of a damaged aircraft wing under static loads. A comparison was made of calculated and experimentally measured strains on primary structural components of an RF-84F wing. This comparison brought out two sensitive areas in modeling semimonocoque structures. The calculated strains were strongly affected by the type of elements used adjacent to the damaged region and by the choice of MPC (multipoint constraints) sets on the damaged boundary.

DESCRIPTION OF STRUCTURE

Left wings from RF-84F aircraft were tested in this program. This fighter, designed for high subsonic speeds, had a wing span of 10 m. Its loaded weight was approximately 11 Mg. The wings were two-spar semimonocoque structures with the quarter-chord line swept back at 40 degrees. Both spars and four major ribs in each wing were aluminum forgings. Three outboard ribs were built up from extrusions. This basic framework (Figure 1) was covered by stringers and a skin of sheet aluminum. The entire structure was composed of 7075-T6 material with the exception of a few 2024-T3 skin panels.

An undamaged wing and five damaged wings were tested. The extent and location of damage for three of the wings are illustrated. (For example, see Figure 2.) These three cases had substantial damage to either the front or rear spar, a condition that previously caused large differences between predicted and measured strains (ref. 1). The damage cases investigated were all roughly 0.6-m diameter holes at 40 percent of the wing span. The damaged areas were cut out of the wings with a welding torch. Burned edges were ground back about 1 cm to reduce the heat-affected zone. In each of the three cases shown,

damage reduced the area moment-of-inertia of the wing about a chord line passing through the damaged region by 10 to 15 percent.

STATIC LOADING TESTS

The wings were cantilevered horizontally from a test fixture by their mounting lugs. Hydraulic jacks located at B and C in Figure 1 provided a static vertical force. Eighty-five percent of the force was applied to the front spar and fifteen percent to the rear spar to simulate a load distribution due to aerodynamic lift. With the undamaged wing, a 45-kN force applied in this way resulted in a uniform deflection of approximately 15 cm at the wing tip. With the damaged wings, deflections at the point of load application sometimes exceeded the 30-cm stroke of the jacks before failure. When this happened the wings were supported in the deformed configuration while the load was removed from the jack for shimming. Elimination of strain relaxation during shimming was a goal. In three tests where damage had been done to the main spar, the loads were slowly increased until failure occurred. In the other three tests, limitations of the test fixture prevented forces large enough to cause failure from being applied.

In these tests strains were measured at eight locations on major structural elements of the wings. The location of four pairs of SR4 strain gages is shown on Figure 1. These gages were mounted parallel to the spar axis on the top and bottom of the spar caps. In most cases, measured strains were linear up to failure since the gages were not near the critical section (ref. 1). Gages near where failure occurred (particularly 3 and 4) recorded nonlinear strains at loads as small as 50 percent of maximum. The measured strain data shown for a 45-kN load were determined by extrapolation of data from the 9 kN-to 27-kN range. At these lower load levels the data were linear, hence comparable with a linear theoretical analysis.

ANALYTICAL MODEL DEVELOPMENT

Element Selection

A finite element model of the RF-84F wing structure was developed based on measurements made in the field. The first model (A in Figure 3) used simple elements in the interest of economy. ROD and SHEAR elements represented the spars. The skin in Model A is composed of quadrilateral SHEAR elements that are bordered by ROD's representing both stringers and in-plane skin stiffness. This model had about 250 degrees-of-freedom.

In this structure, the spars carry most of the bending loads. The ROD elements representing bending stiffness of the spars were located on the wing surface. Their cross-sectional area was chosen to provide the correct moment-of-inertia for each spar about its centroid. This representation resulted in a cross-sectional area for the model that was smaller than that of the structure. Since the cross-sectional area of the spar and its model were not the same, stresses caused by axial loads were not correct. Stresses on the wing surfaces caused by bending loads were correct when a principal axis of inertia for the wing cross-section passed through the spar centroid. Generally, the bending stiffness of a model created in this way would be somewhat smaller than the stiffness of the structure. In these wings, this influence of modeling technique was less than 5 percent.

The later Model C (Figure 4) varied from A in two respects: the number of elements was increased and in-plane stiffness was retained in the skin elements. After introducing additional grid points along the wing, elements in the three large bays were made one-half their original length. This increased the problem size to 340 degrees-of-freedom. Further, the SHEAR elements that represent skin in Model A were replaced by TRMEM elements. These smaller elements with wider load carrying capability were expected to improve load distribution around damaged regions.

Although the strains predicted by these models were reasonable for the undamaged structure, they compared very poorly with measured values when either spar was damaged. In these cases of damage, differences were as large as an order of magnitude. Consequently, the structural representation around the damaged region was reconsidered. The simple ROD and SHEAR elements representing beams were found to be inadequate for the complex load distribution in the vicinity of damage. In damage cases 2 and 5 where half of the beam was removed over a 76-cm length, the ROD representing the residual spar section was replaced by BEAM elements through the damaged region. MPC's were required at the ends of these elements to enforce compatibility with the slope of adjacent structure. In damage case 3 where the rear spar was cut completely, the bending forces carried by that spar were transferred to the short intermediate spar. The transfer occurred mainly through ribs at each end of the intermediate spar. Hence, torsional stiffness of the ribs became important and was added to the properties of the ROD elements representing these components. Twist in the ribs was determined by MPC's relating relative displacements of top and bottom grid points. These local modifications to the analytical model greatly improved the correlation of analytical and experimental results.

Constraints Around Holes

The simple structural elements used in the analytical model require special consideration on free boundaries. When elements are removed to represent damage, grid points bordering the hole can be left with

unrestrained degrees of freedom. A fatal error due to grid point singularity will result. This can be remedied by providing displacement constraints on these grid points by means of multipoint constraints. The choice of constraint conditions is not unique. It is easy to specify large displacements that are not compatible with the free edge of a hole. Forces required to achieve MPC constraints are not output directly so the degree of compatibility is not easily checked. Equilibrium considerations on free body sections passing through the hole can be used to determine these forces. Comparison with element forces at the cross-section has been used to test how well an MPC set satisfies the stress-free boundary condition of a hole. Generally, insignificant boundary forces have resulted from specifying a rigid body displacement relative to spanwise adjacent grid points.

COMPARISON OF MEASURED AND CALCULATED STRAINS

For comparison with the experimental results, a 45 kN static force was applied normal to the midplane of the model wing. Of the total, 85 percent was applied at point B of Figure 1 and 15 percent at point C. Stresses in the elements and nodal displacements were calculated using the NASTRAN static analysis rigid format.

Comparisons of calculated and measured strains on the undamaged wing encouraged confidence in the model that was first developed. With both Model A and Model C, calculated strains were within 17 percent of measured values for all gage locations on the undamaged wing. Hence, the large differences that occurred in damaged wings - in some cases as large as an order of magnitude - were a surprise. Since these large differences were only present when the spars were damaged, it first seemed that the skin structure in the vicinity of the damage must be carrying large strain gradients and significant in-plane loads. Models B and C were developed to deal with these possibilities. They had a smaller element size and membrane rather than shear elements. These models did not substantially improve the correlation of analytical and experimental results (compare ROD models in Figures 5 and 6). Subsequently, the simple elements adjacent to damage were replaced by higher order elements that could also carry bending or torsional loads. This markedly improved the correlation of calculated and measured strains.

Spar strains calculated by the analytical models are compared with the few measured values in Figures 5 and 6. Figure 7 illustrates damage to the rear spar while Figure 8 shows the measured and calculated strains with this damage. Similarly, Figures 9 and 10 illustrate damage to the underside of the front spar and corresponding strains. These axial strains are along the top and bottom of the front and rear spars on a wing subject to a 45-kN vertical force near the wing tip. In each case of damage to a spar and with both models A and C, the introduction of higher order

elements (H.O.E.) adjacent to damage greatly improved correlation with measured values. This improvement was a result of developing a numerically stable analytical model rather than refinements in the model.

Numerical stability problems are associated with ill-conditioning of the stiffness matrix. In NASTRAN, an index of this problem is the residual load vector,

$$\{\delta P_\ell\} = [I - KK^{-1}]\{P_\ell\}$$

where [I] is the identity matrix, [KK] is a stiffness matrix, and $\{P_\ell\}$ is the applied load vector. A nondimensional index can be defined as the error vector

$$\{\varepsilon\} = \{\delta P_\ell\} / ||\{P_\ell\}||$$

where $||\{P_\ell\}||$ is the norm of the applied load vector. For this wing, comparable results were obtained from the model when all components of $\{\varepsilon\}$ were less than 10^{-14}. A component of the order of 10^{-12} or larger indicated poor modeling. The largest component of $\{\varepsilon\}$ has been shown in Figures 5, 6, 8 and 10 for each model. Another indication of numerical problems caused by poor modeling was the large jump in nodal displacements across the damaged region. Displacements normal to the wing surface just outboard of damage were as large as 25 m. Replacement of elements around damage by higher order elements cured the conditioning problem.

CONCLUSIONS

Large differences between calculated and measured strains in damaged wings have been associated with numerical instability. This was caused by the simple elements initially used to represent structure adjacent to the damaged region. Load distribution around damage was significantly affected by the stiffness of adjacent structural components in planes that had only negligible loads in the undamaged structure. The simple elements provided no stiffness in these planes. More complex elements were required to handle the unusual loads around the damaged region.

Analyses of semimonocoque structures are sensitive to structural discontinuities. Holes and cutouts in particular can be troublesome. The considerations which greatly improved the accuracy of this damaged wing analysis are believed to be generally applicable.

REFERENCE

1. Stronge, W. J.: Failure Prediction for Damaged Aircraft Wings. Proceedings of the Fifth Navy-NASTRAN Colloquium, NSRDC, 1974.

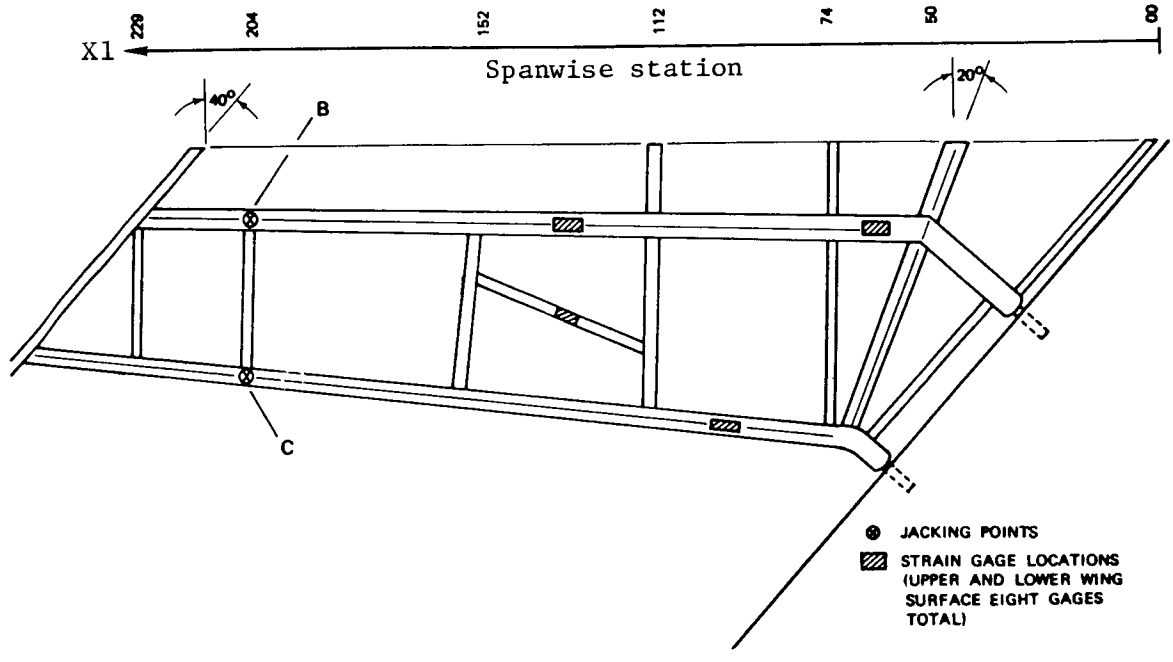

Figure 1.- F84 wing spars and ribs.

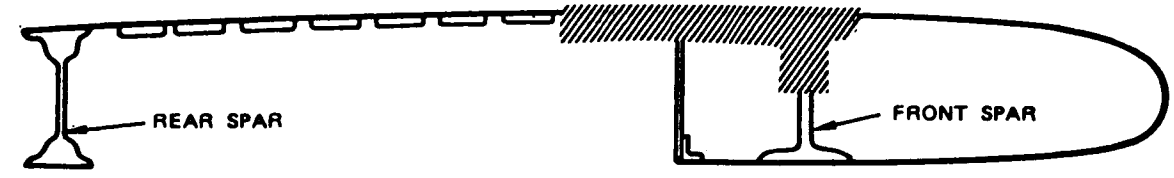

SECTION A–A

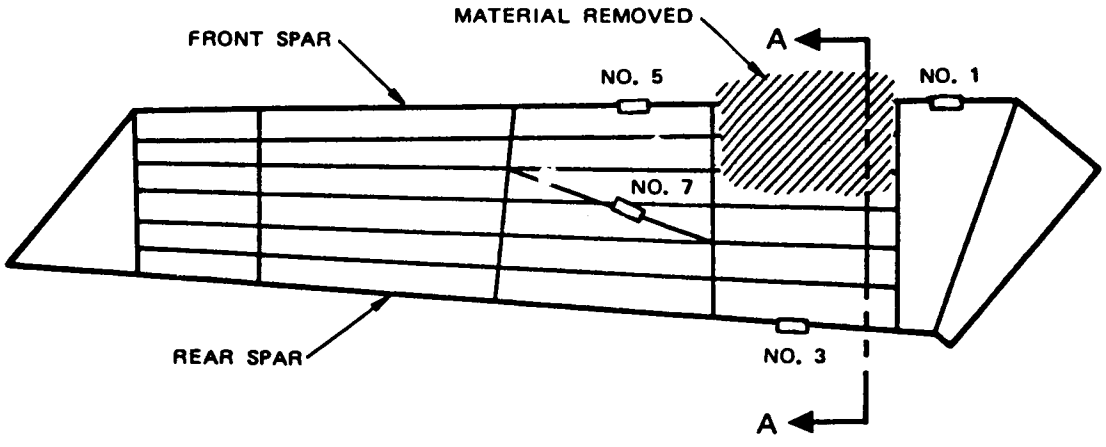

Figure 2.- Wing no. 2.

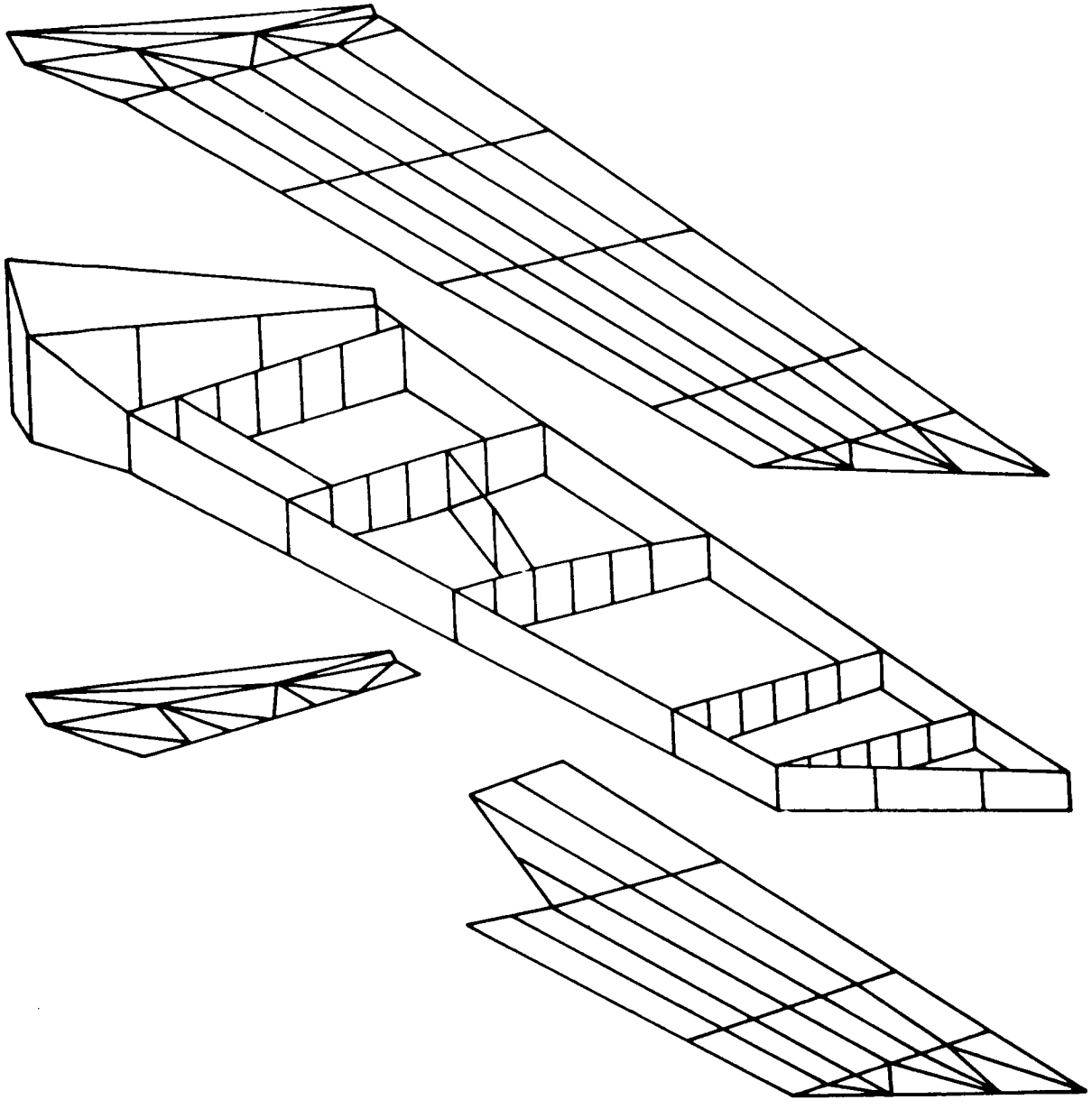

Figure 3.- Model A.

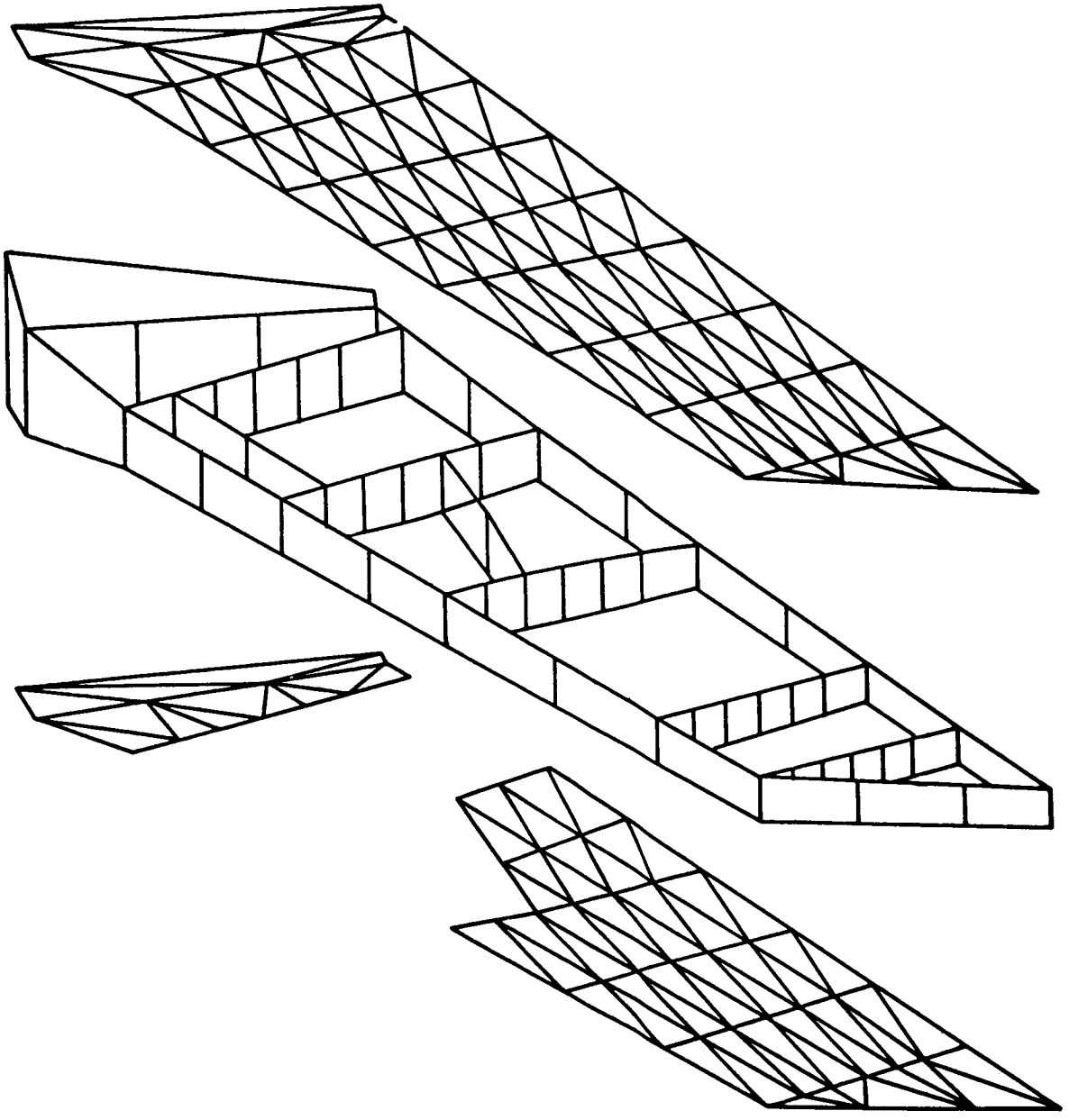

Figure 4.- Model C.

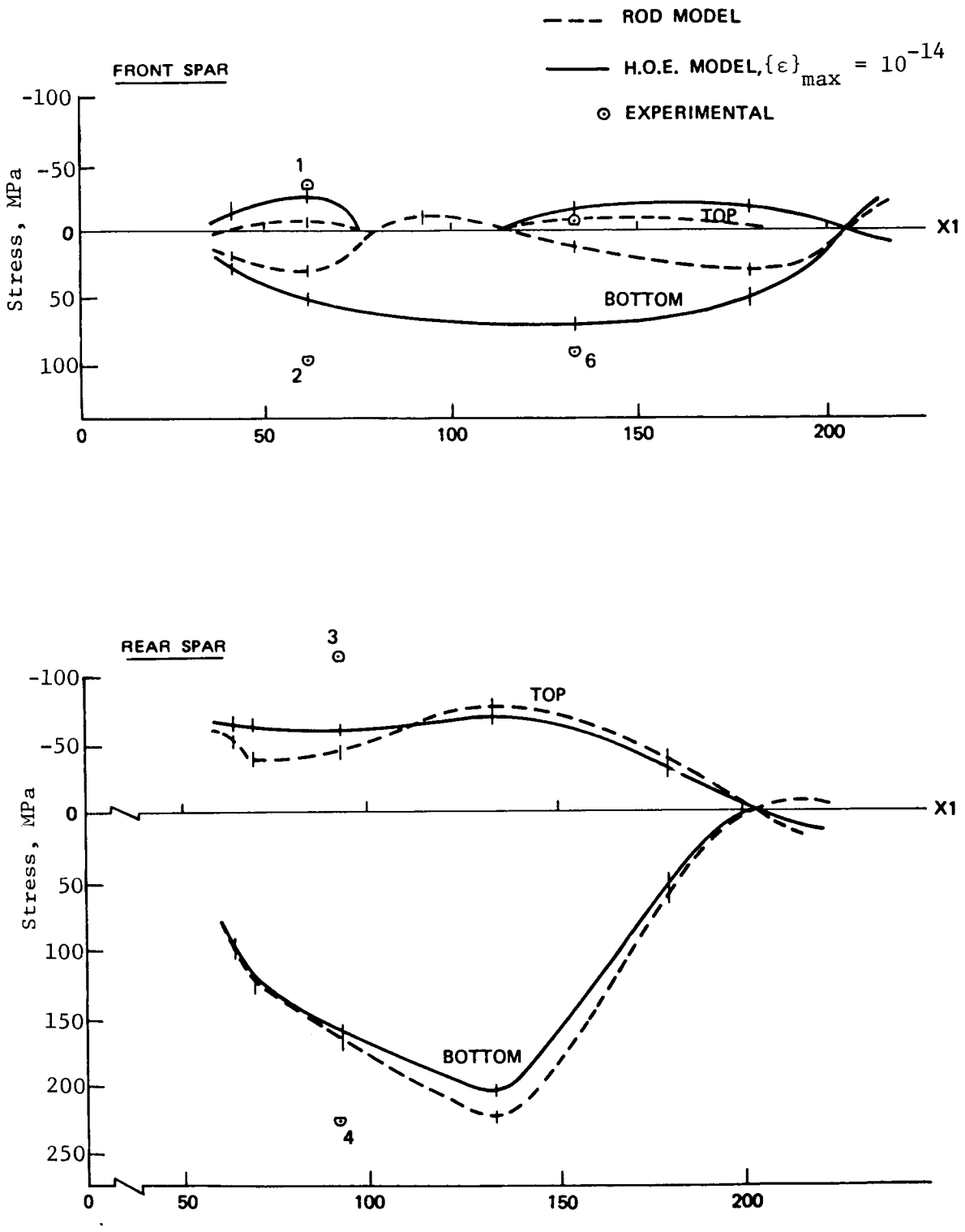

Figure 5.- Damage no. 2, model A.

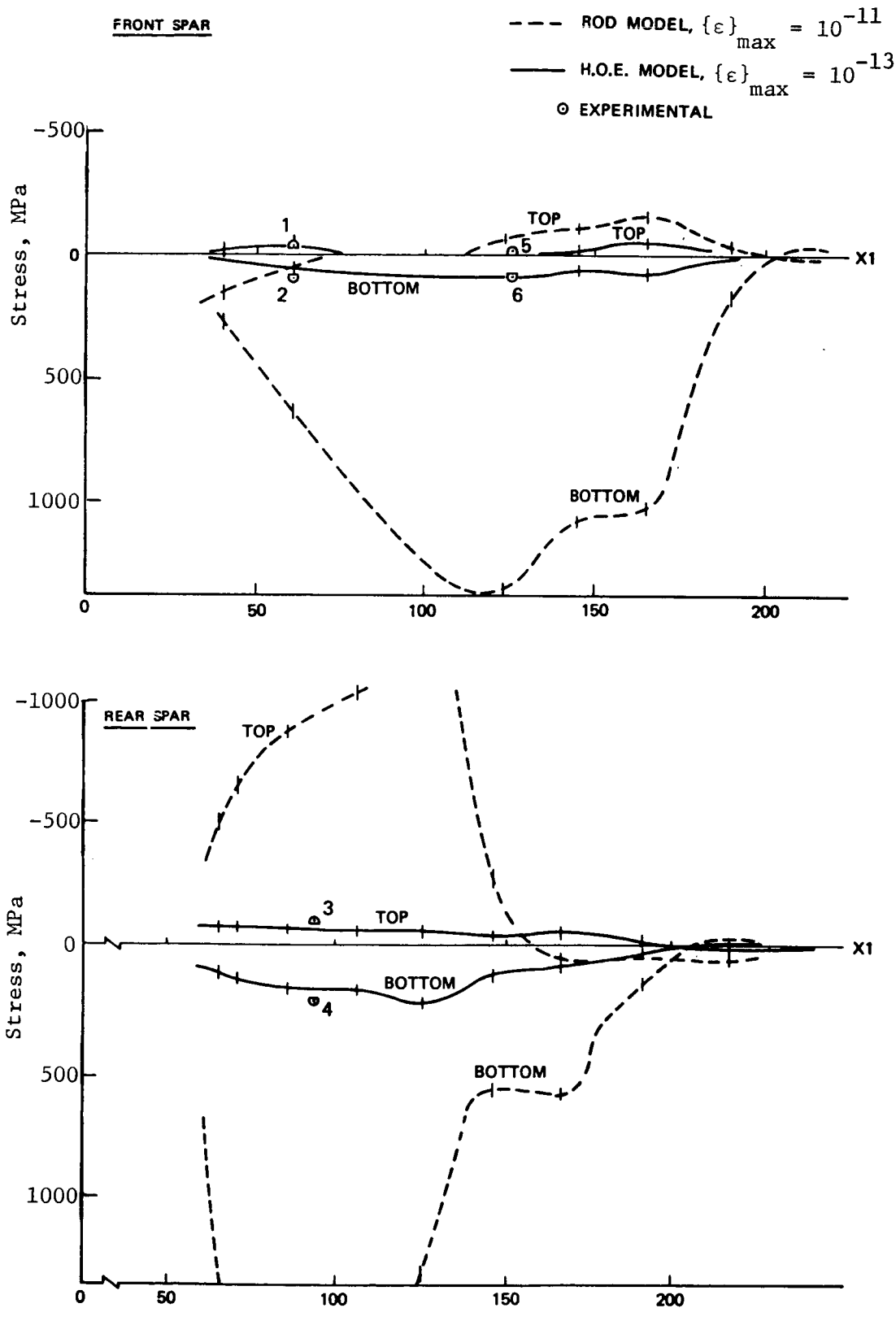

Figure 6.- Damage no. 2, model C.

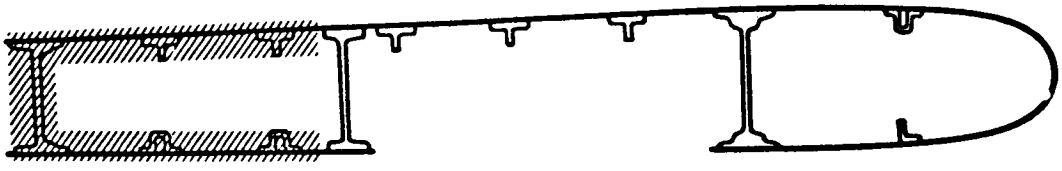

SECTION A–A

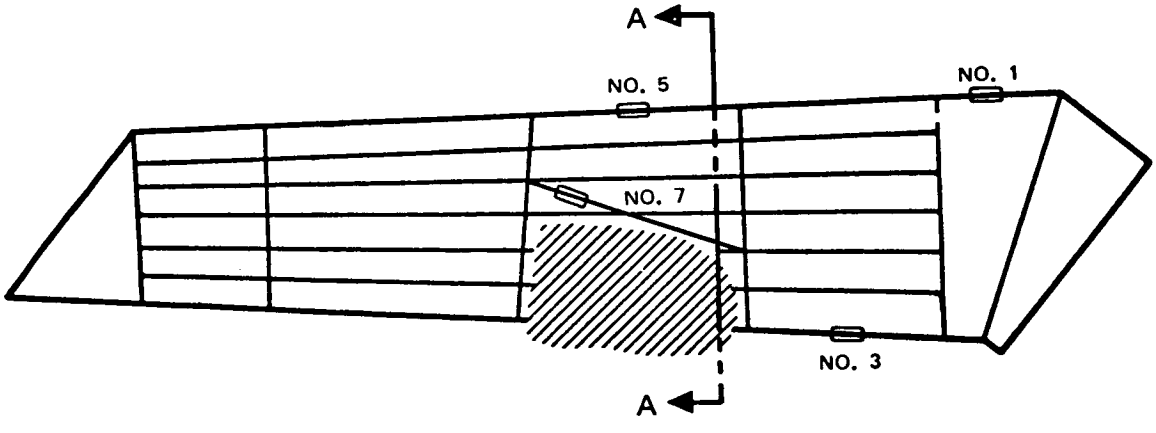

Figure 7.- Wing no. 3.

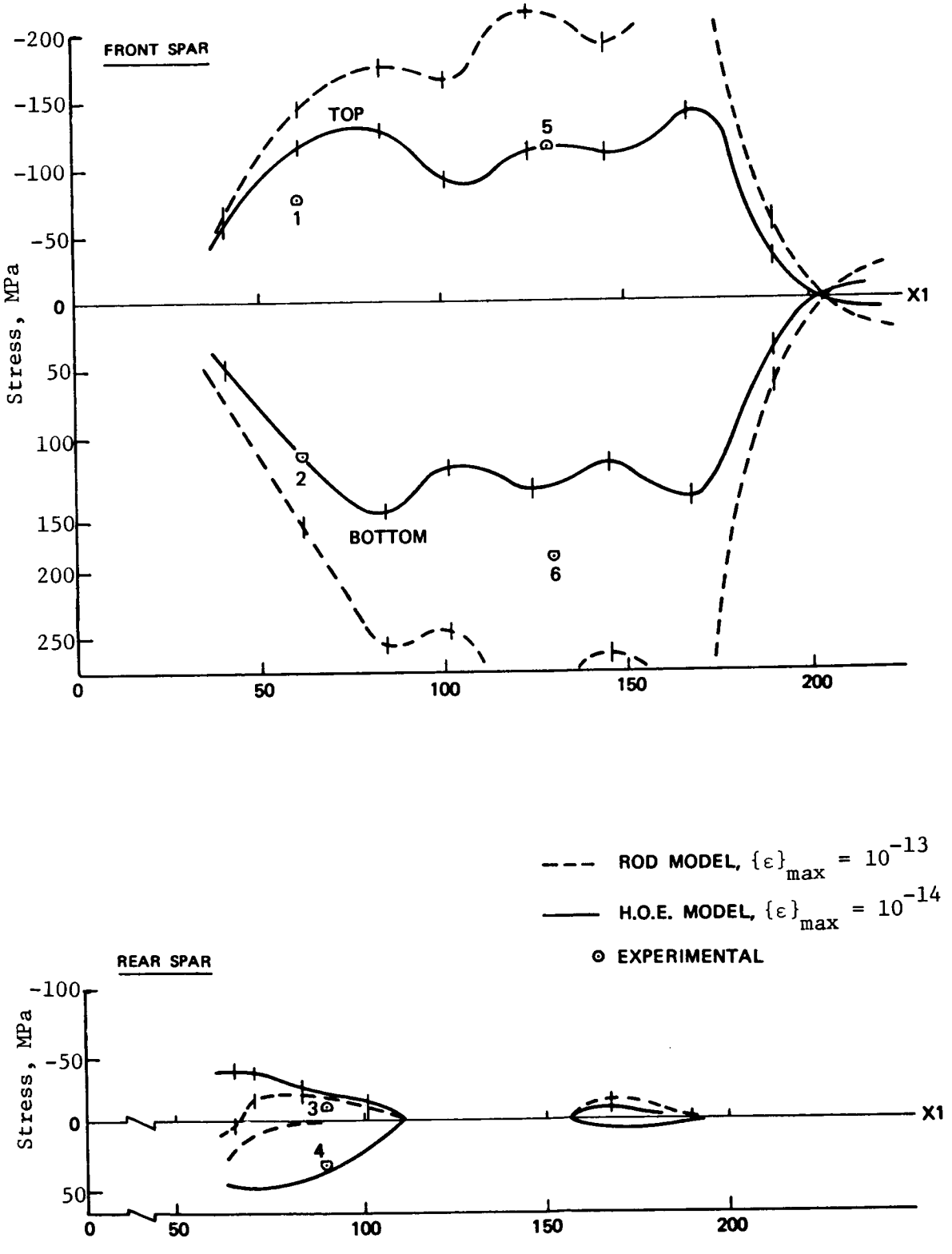

Figure 8.- Damage no. 3, model C.

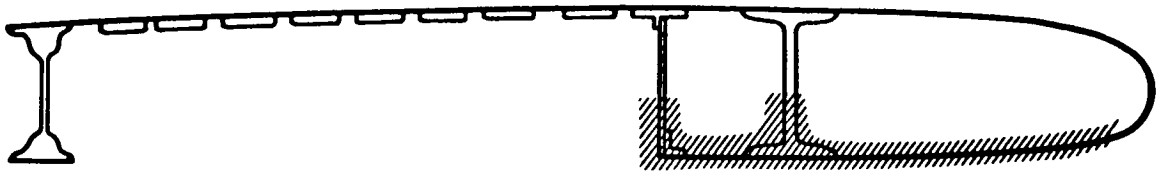

SECTION A–A

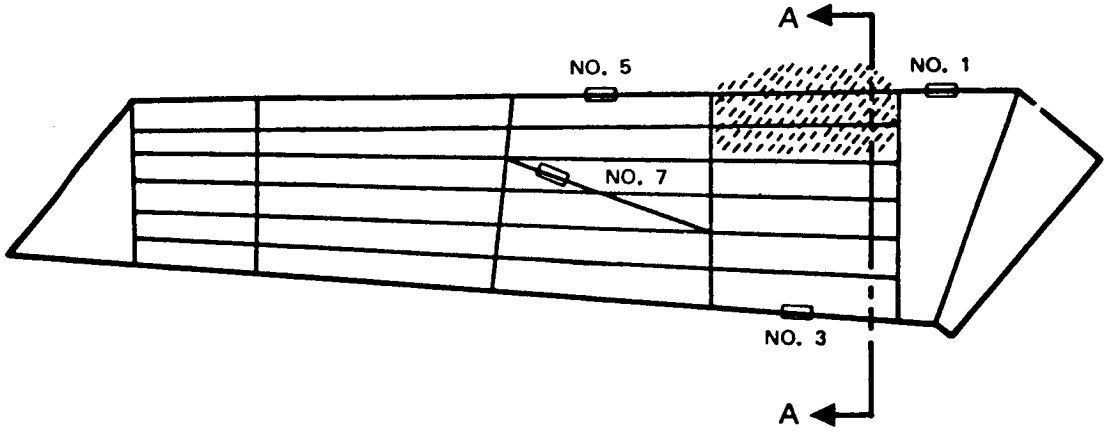

Figure 9.- Wing no. 5.

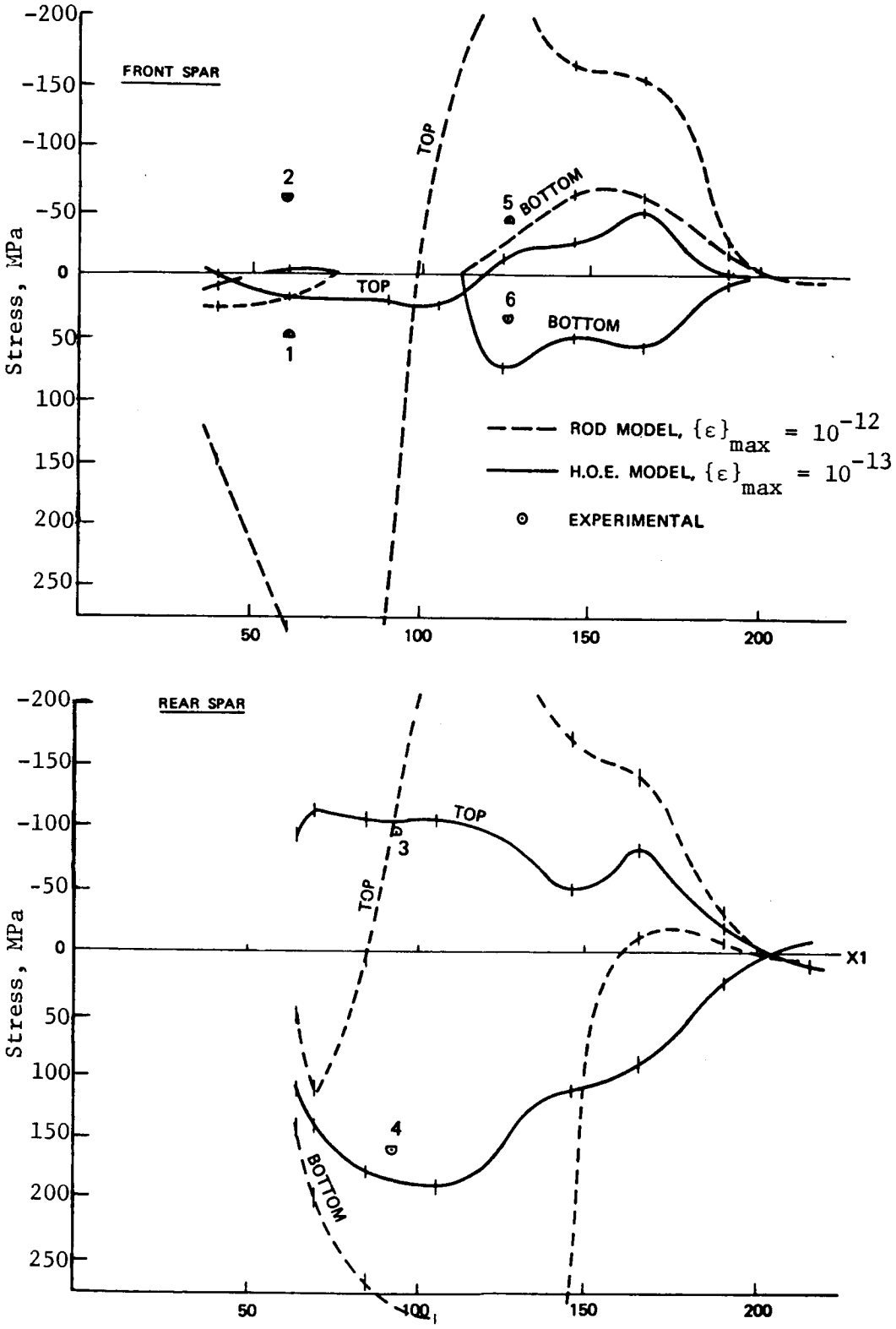

Figure 10.- Damage no. 5, model C.